

光学学报

基于后验误差分析的多角度偏振成像仪 气溶胶反演测试

王涵^{1*}, 孙晓兵², 赵梅如^{3**}, 秦凯¹

¹中国矿业大学环境与测绘学院, 江苏 徐州 221116;

²中国科学院安徽光学精密机械研究所, 安徽 合肥 230031;

³安徽师范大学地理与旅游学院, 安徽 芜湖 241000

摘要 通过分析多角度偏振成像仪(DPC)的后验误差, 测试DPC的气溶胶反演效果, 为算法改进提供支持。使用GRASP (generalized retrieval of aerosol and surface properties) 算法在同等条件下对DPC和POLDER(polarization and directionality of the earth's reflectance)数据进行反演, 分析两种传感器的强度(RI)和偏振(RP)的反演残差及气溶胶光学厚度(AOD)误差; 讨论山区和非山区AOD的反演精度及加入偏振信息对反演的改进。在多数波段, DPC的AOD反演精度接近POLDER, 但在865 nm波段二者有较大正向偏差; RI@565、RI@865及RP@865的绝对值较大且较为离散; 非山区上空DPC与POLDER反演精度接近, 但在山区二者均出现系统性偏高, DPC尤为明显; 偏振信息的加入可以有效改善仅强度条件下的反演结果; 扣除干扰因素, 非山区上空AOD@670落入期望误差范围的比例为63.7%, 相关系数为0.828。

关键词 遥感与传感器; 气溶胶; 偏振; 多角度偏振成像仪

中图分类号 P407.4

文献标志码 A

DOI: 10.3788/AOS230569

1 引言

气溶胶是地球大气系统的重要组成部分, 对辐射强迫^[1]、气象^[2]、环境^[3]、定量遥感^[4]以及人类健康^[5]有重大影响。科学的研究及社会生产生活对高精度气溶胶产品的需求持续增长^[6]。

在基于强度信息的遥感基础上, 多光谱、多角度和偏振的多维观测可以更好地实现全球气溶胶探测。分别搭载ADEOS-1(1996年)、ADEOS-2(2002年)和PARASOL(2004年)卫星的POLDER(polarization and directionality of the earth's reflectance)系列传感器是其中代表, 推动了气溶胶遥感及相关传感器的研究。POLDER-1和POLDER-2在轨运行时间较短, POLDER-3运行超过8年时间, 因此被广泛使用(本研究采用的即为POLDER-3数据, 后文简称POLDER)。POLDER可以提供3个偏振波段、6个非偏振波段以及所有波段最多14个角度的观测数据。早期的气溶胶偏振反演算法基于气溶胶和地表类型的设定实现了海洋和陆地上空的气溶胶反演^[7-8]。段民征等^[9]也开展了同时反演POLDER多维观测的气溶胶和地表反照率的研究。随着地表强度/偏振双向反射分布函数(BRDF/BPDF)半经验模型^[10-12]的发展, GRASP

(generalized retrieval of aerosol and surface properties) 算法^[13] 和 SRON (Netherlands Institute for space research) 算法^[14] 实现了使用多维数据同时反演地/海表反射模型参数和气溶胶光学与微物理特性参数。国内也陆续开展了基于POLDER强度和偏振信息的气溶胶遥感研究, 实现了气溶胶光学厚度(AOD)和细粒子比^[15]、气溶胶类型^[16] 及粒子谱分布^[17] 反演。此外, APS (aerosol polarimetry sensor)、POSP (particulate observing scanning polarimeter)、CAPI (cloud and aerosol polarimetric imager)、MAI (multi-angle polarization imager)、3MI (multi-view multi-channel multi-polarization imaging mission) 和 HARP (hyper-angular rainbow polarimeter) 等已运行和计划运行的传感器也为偏振遥感的发展提供了支撑, 进而使基于多维观测数据的气溶胶反演算法的需求增加^[18]。

多角度偏振成像仪(DPC)传感器是我国用于全球云和气溶胶观测而开发的, 最早用于航空观测, 于21世纪初研制成功, 并实现了区域气溶胶观测^[19]。用于卫星观测的DPC分别搭载高分五号01星(2018年)、02星(2021年)和大气环境监测卫星(2022年)开展全球大气环境监测。本研究所用数据来自高分五号02星上的DPC-2传感器(后文简称DPC), 可以获取3

收稿日期: 2023-02-20; 修回日期: 2023-03-22; 录用日期: 2023-04-13; 网络首发日期: 2023-05-08

基金项目: 国家自然科学基金(42075132)

通信作者: *ms.h.wang@cumt.edu.cn; **zhaomr_cc@163.com

个偏振波段及5个非偏振波段,最多17个角度的观测数据。郑逢勋等^[20]对DPC反演结果后验误差的影响因素进行了模拟分析;Li等^[21]使用DPC偏振数据反演了细模态AOD,并绘制了全球最高分辨率的雾霾地图;Wang等^[22]使用DPC数据初步反演了典型区域的AOD和Angstrom指数(AE)。目前依然迫切需要DPC提供可靠的科学级和应用级的气溶胶产品。针对反演结果后验误差的分析是测试DPC性能的一个重要手段。本文使用GRASP反演算法,对DPC的反演结果进行误差分析,通过与POLDER反演效果对比,分析气溶胶反演误差对波段和散射角的依赖关系,讨论山区和偏振信息对DPC反演的影响,测试DPC在气溶胶遥感方面的能力。

2 数据与测试流程

2.1 数据

测试分析所用的数据包括DPC与POLDER的卫星观测数据以及AERONET(aerosol robotic network)

表1 DPC反演测试所需数据说明

Table 1 Description of data used in DPC inversion test

| Data source | Data level | Collection time | Parameter |
|-------------|------------|-----------------|--|
| DPC | L1 | 2022 | Multi-spectral intensity and polarized reflectance, observation geometry, and so on. |
| POLDER | L1 | 2012 | |
| AERONET | Level 2.0 | 2012 and 2022 | Multi-spectral AODs |

2.2 测试流程

整个流程经过数据匹配和反演,从波段和散射角两方面开展分析,并与POLDER在同等条件下进行对比。

1)数据匹配

为了提升测试效率,需要将卫星数据与地基数据进行时空匹配、裁剪和存储,后续计算均以此为基础。首先,确定AERONET站点上空卫星过境时间,然后确定AERONET站点所在像元;选取卫星过境前后各30 min内的AERONET数据,如果时间区间内的数据超过一条,取AOD平均值存储;同时以AERONET站点所在像元为中心裁剪出相应邻域(由于DPC与POLDER空间分辨率不同,DPC选取5×5邻域,POLDER选取3×3邻域,从而使二者反演结果的空间分辨率接近)。此外,气溶胶反演精度会受山区地表起伏影响^[23],因此,将匹配数据按照山区和非山区分别进行分析。依据《1:5000 1:10000地形图航空摄影测量外业规范》(GB/T 13977—2012)中的地形类别划分标准,选择25 km范围内地面倾角大于2°、海拔落差大于20 m的区域作为山区,其他为非山区。根据POLDER和DPC在轨运行时间选择了2012年POLDER和2022年DPC的观测数据进行测试和对比,最终分别成功匹配了1591条(其中山区463条)及1483条(其中山区408条)数据。

地基数据,所用数据的细节信息如表1所示。POLDER的空间分辨率约为5.3 km×6.2 km,在运行期间可以提供超过9年的多光谱、多角度的偏振波段(490、670、865 nm)和非偏振波段(443、565、763、765、910、1020 nm)观测数据。目前高分五号02星所搭载的DPC已经在轨运行超过一年,可以提供稳定数据,其空间分辨率约为3.5 km×3.5 km,可以获取3个偏振波段(490、670、865 nm)、5个非偏振波段(443、565、763、765、910 nm)以及所有波段最多17个角度的观测数据。在测试过程中,需要使用DPC和POLDER的L1级产品数据,数据包括各波段表观反射率、观测几何关系、海陆标记、经纬度等。AERONET采用地面太阳光度计进行大气参数测量,通过测量可见光至近红外波段范围内一系列波段大气对太阳直接辐射的消光系数及天空光,可提供范围为0.34~1.06 μm的AOD数据及其他光学与微物理特性数据。本研究采用AERONET Level 2.0数据中的AOD作为验证标准值。

2)气溶胶反演

利用GRASP算法反演已匹配的DPC与POLDER数据,反演程序由GRASP-OPEN(<https://www.grasp-open.com/>)提供。在反演过程中采用multi-pixel模式,地表强度和偏振反射分别采用Ross_Li BRDF和Maignan BPDF模型^[10-11],气溶胶参数由初始估计和先验知识约束。为了测试DPC的反演性能,确保在同等条件下进行对比:①没有直接采用GRASP发布的POLDER反演产品,而是同时开展DPC与POLDER数据的反演;②在反演过程中,只采用DPC与POLDER共同的波段,即443、490、565、670、865 nm(去除用于探测云顶氧压的763、765 nm波段)。

3)波段因素分析

应用于DPC和POLDER反演的GRASP算法可以提供多波段的气溶胶光学特性参数(包括AOD、AE、单次散射反照率等)、微物理特性参数(包括复折射指数、谱分布等)以及地表特性参数。利用SOS(successive order of scattering)^[24]辐射传输程序,以DPC和POLDER的反演结果作为输入开展正向模拟,得到强度与偏振表观反射率,与观测值对比得到各波段、各角度的反演残差(RI和RP分别表示强度和偏振残差)。由于GRASP产品中只提供总的反演残差,这里使用SOS重新进行计算以得到多波段和多角度

的残差分布。在此基础上分析各波段 RI 和 RP 的分布情况;然后,以 AERONET 观测的多波段 AOD 为标准,在同等条件下对比 DPC 和 POLDER 反演的 AOD 相对 AERONET 产品的误差分布差异。

4)角度因素分析

卫星观测散射角多数分布在 $100^\circ \sim 175^\circ$ 之间,按照 5° 间隔研究 RI 和 RP 的分布情况,以分析散射角对 RI 和 RP 的影响。由于角度受地形影响明显,按照山区和非山区分别开展分析,并与 POLDER 在同等条件下进行对比。因此,分别开展 RI 和 RP 的散射角依赖以及山区与非山区的对比分析。

3 结 果

3.1 波 段

RI 和 RP 的波段分布如图 1 所示,图 1(a)、(b)分

别对应 DPC 和 POLDER。从图 1 可以看出:1)DPC 与 POLDER 的 RI 和 RP 均处在较低水平,分别在 10×10^{-3} 和 10×10^{-4} 上下;2)从误差棒(标准差)来看,DPC 与 POLDER 的 RI 和 RP 总体分布较为集中,但是对 DPC 来说,RI@565、RI@865 以及 RP@865 的误差棒较大,分布较为离散。

为了更直观地展示反演结果的误差情况,将各个波段反演的 AOD 与对应的 AERONET 观测结果进行统计对比。由于 AERONET 与 DPC 和 POLDER 波段并不严格一致,需要将 AERONET 观测的 AOD 转换到与 DPC 和 POLDER 对应的波段上,表示为

$$\ln[\tau(\lambda)] = a + b \ln \lambda + c \ln \lambda^2, \quad (1)$$

式中: $\tau(\lambda)$ 为 λ 波段的 AOD; a 、 b 和 c 为拟合系数,通过 AERONET 多波段 AOD 可以拟合得到对应系数。通过式(1)可以实现精确拟合,误差小于 0.02^[25]。

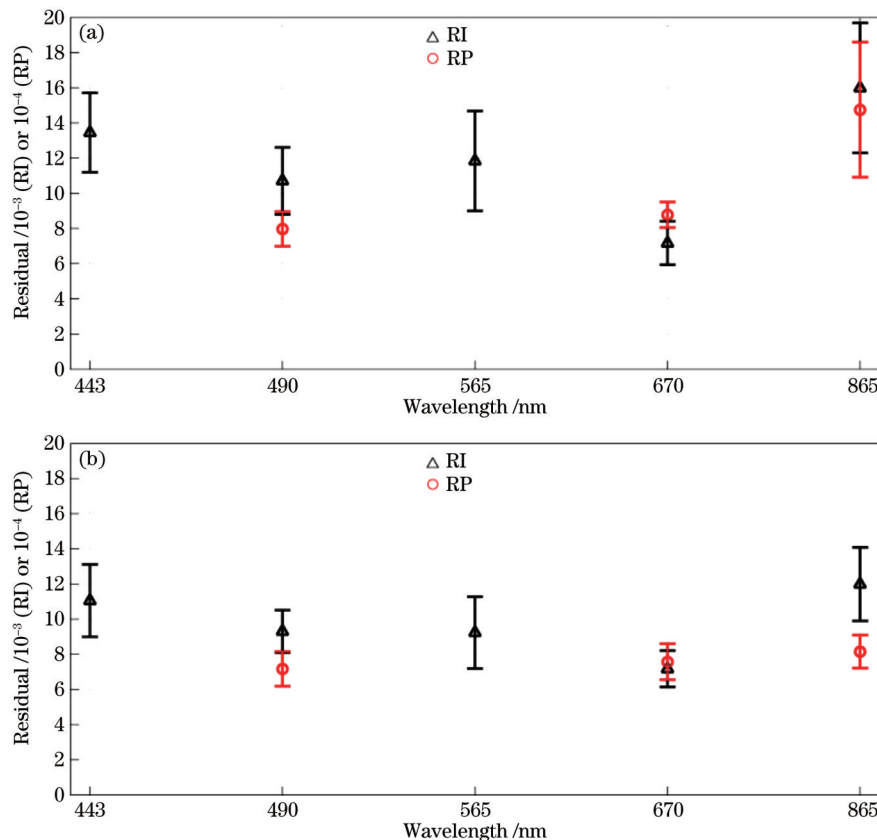


图 1 反演残差的波段分布。(a)DPC;(b)POLDER

Fig. 1 Wavelength dependences of retrieval residuals. (a) DPC; (b) POLDER

利用多个统计数据分别对 DPC 和 POLDER 相应波段的 AOD 与 AERONET 结果进行误差分析,包括拟合直线的斜率(k)、观测均值(mean value)、平均偏差(mean bias)、相关系数(R)、均方根误差(RMSE)以及期望误差区间($R_{EE} = 0.05 + 0.15\tau$,其中 τ 为 AERONET 观测结果)分布百分比,结果如表 2 所示。可以看出:1)POLDER 总体表现较为稳定,反演结果较好,可以作为 DPC 的参考对象;2)DPC 的反演结果

总体上与 AERONET 一致性较高,体现了 DPC 在气溶胶观测方面的能力;3)DPC 除 865 nm 波段拟合斜率为 1.28,其他波段拟合斜率均接近于 1;4)除 865 nm 波段外的 mean value 能反映出 AOD 的波段变化规律;5)mean bias 均为正值,反映了反演结果有一定程度的正系统偏差;6)所有波段的相关系数均较高,RMSE 也处在合理范围内;7)DPC 中,AOD@865 在 within R_{EE} 范围内的比例较低,而在 above R_{EE} 范围内的比例过

高,表明 AOD@865 严重偏高;8)DPC 各个波段处在 above R_{EE} 的比例普遍高于处在 below R_{EE} 的比例,也表明了反演结果存在普遍高估的情况。综合拟合斜率和

期望误差区间分布百分比,DPC 的 865 nm 波段的 AOD 被严重高估而其他波段不存在这种现象,这应该与 DPC 的 L1 级数据有关。

表 2 各波段对应的 DPC 与 POLDER AOD 反演结果统计参数
Table 2 Statistical parameters from DPC and POLDER retrieved AODs at different wavelengths

| Sensor | DPC | | | | | POLDER | | | | |
|---------------------|-------|-------|-------|-------|-------|--------|-------|-------|-------|-------|
| Wavelength / nm | 443 | 490 | 565 | 670 | 865 | 443 | 490 | 565 | 670 | 865 |
| k | 1.02 | 0.93 | 0.88 | 0.99 | 1.28 | 0.91 | 0.89 | 0.95 | 1.02 | 1.05 |
| Mean value | 0.33 | 0.28 | 0.26 | 0.21 | 0.28 | 0.35 | 0.29 | 0.24 | 0.21 | 0.18 |
| Mean bias | 0.095 | 0.044 | 0.069 | 0.052 | 0.112 | 0.087 | 0.075 | 0.062 | 0.034 | 0.041 |
| R | 0.81 | 0.85 | 0.83 | 0.84 | 0.81 | 0.89 | 0.88 | 0.87 | 0.89 | 0.91 |
| RMSE | 0.25 | 0.21 | 0.20 | 0.16 | 0.23 | 0.24 | 0.19 | 0.19 | 0.18 | 0.15 |
| Within R_{EE} / % | 45.02 | 51.18 | 50.50 | 53.99 | 31.33 | 48.73 | 58.46 | 55.56 | 60.96 | 59.58 |
| Above R_{EE} / % | 39.83 | 33.08 | 23.47 | 30.17 | 53.04 | 33.18 | 29.82 | 33.05 | 25.05 | 24.16 |
| Below R_{EE} / % | 15.15 | 15.74 | 26.03 | 15.84 | 15.63 | 18.09 | 11.72 | 11.39 | 13.99 | 16.26 |

3.2 散射角

按照散射角分布情况对 RI 和 RP 进行分析,以研究残差与散射角的相关关系。由于小于 100° 和大于 175° 的数据量较少,这里对在 100°~175° 范围内以每 5° 为一个区间的散射角开展分析。同时由于地形条件对观测影响较大,在分析过程中按照山区和非山区(包括城区)分别开展残差对比,结果如图 2(非山区)和图 3(山区)所示。从图 2、3 可以看出:1)山区的 RI 和 RP

均值高于非山区,且分布较为离散,说明由于山区地形起伏而产生的观测几何关系、地气耦合等因素对气溶胶反演结果的影响较大;2)非山区的 RI 和 RP 均较为集中,但是在散射角较大的情况下(大于 160°)标准差较大,表明大散射角情况下出现了 RI 和 RP 较为离散的情况,这是由于在辐射传输模拟时后向散射会带来较大的误差;3)在非山区,RI 和 RP 随角度变化不大,但山区的 RI 随角度波动较大,RP 较为稳定;4)DPC 与

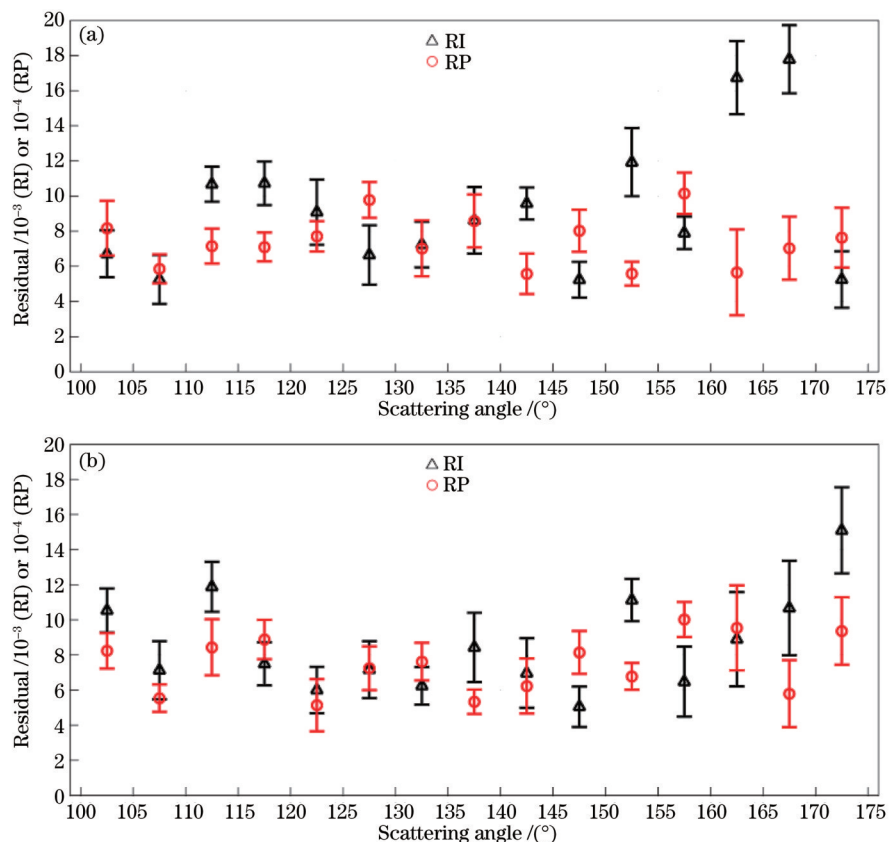


图 2 非山区反演残差的散射角分布。(a)DPC;(b)POLDER
Fig. 2 Scattering angle dependences of retrieval residuals in non-mountain area. (a) DPC; (b) POLDER

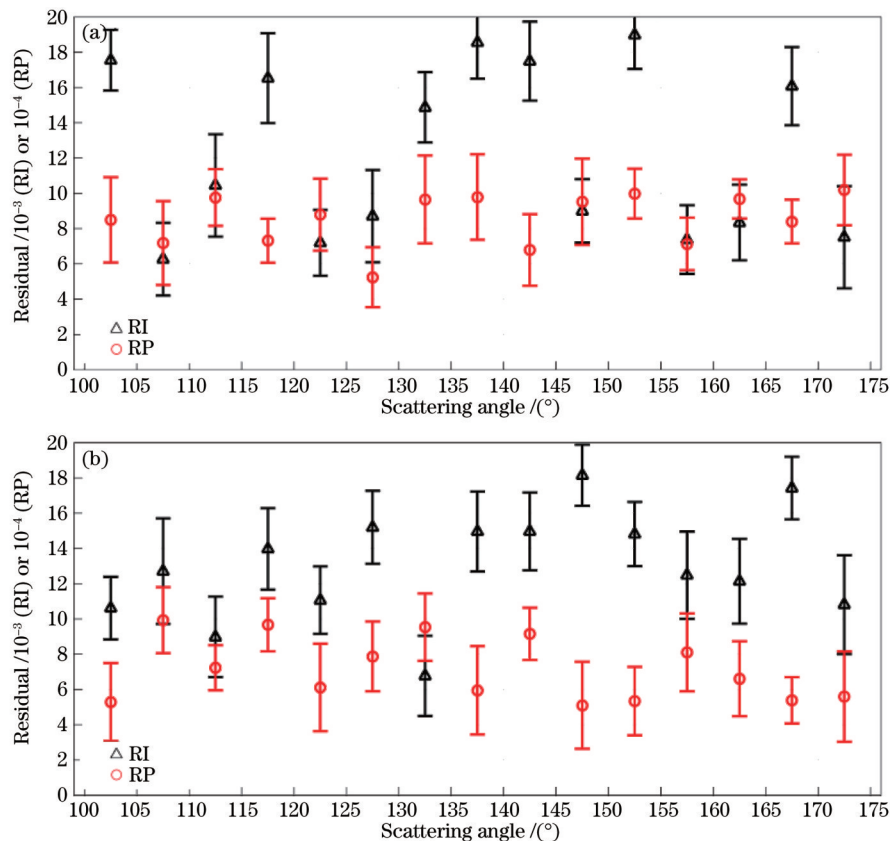


图3 山区反演残差的散射角分布。(a)DPC;(b)POLDER

Fig. 3 Scattering angle dependences of retrieval residuals in mountain area. (a) DPC; (b) POLDER

POLDER 残差的角度特性较为一致,没有明显的差别。

4 讨 论

4.1 山区与非山区反演误差

从 RI 和 RP 的分布可以看出,不论是 DPC 还是 POLDER,在山区均会产生较大的偏差和不确定性。这里从反演 AOD 的误差出发,分析山区与非山区条件下的反演结果,探索山区的复杂条件对 DPC 气溶胶反演结果的影响。从上述分析可以看出,DPC 在 670 nm 波段反演的 AOD 较为稳定,这里利用 AOD@670 开展分析。图 4 是 DPC 和 POLDER 在山区和非山区反演的 AOD 与 AERONET 的反演结果对应的偏差分布曲线和散点分布。从图 4 可以看出:1)反演误差分布近似高斯曲线,中心点在零点附近;2)不论是 DPC 还是 POLDER,山区反演的 AOD 均显著偏高,非山区的反演结果大部分处于期望误差范围内(Within R_{EE} 为 50% 以上);3)在非山区,POLDER 的反演结果从相关系数、RMSE 以及落入期望误差区间的比例来看,均稍微优于 DPC 反演结果;4)在山区,POLDER 落入 R_{EE} 的比例为 42.6%,显著高于 DPC(32.2%)。总体来说,DPC 在非山区的反演能力接近于 POLDER,而在山区落后于 POLDER。由于 DPC 的空间分辨率高于 POLDER,因此,其在山区上空利用 BRDF 和 BPDF

模型开展反演时受地形影响较大。

4.2 偏振对反演结果的改善

从上述分析中发现,大散射角情况下反演结果会产生较大的残差,在山区上空也是如此。为了获取较高的反演精度,下面只使用非山区观测数据,并且把大于 160° 散射角的观测数据扣除,尝试获取 670 nm 波段 DPC 的高精度反演结果。分别分析单一强度(I)反演以及强度与偏振结合(I+P)反演结果,来讨论加入偏振信息对 AOD 反演结果的影响。误差分布和散点分布结果如图 5 所示。从图 5 可以看出,加入偏振信息会使 AOD 反演效果有较大的提升,相关性(0.763 升至 0.808)、RMSE(0.373 降至 0.213)、mean bias(0.117 降至 0.012)、落入 R_{EE} 的比例(44.4% 升至 55.7%)均有所改善。对比图 5(b)和图 4(a)可以看出,在反演过程中扣除大散射角会使反演效果有一定改善,但改善效果并不十分明显。

5 结 论

基于 GRASP 反演算法测试了 DPC 气溶胶反演结果受波段和散射角的影响情况,并讨论了山区与非山区条件下 DPC 的反演能力以及加入偏振信息对反演结果的提升效果。

DPC 在不同波段的残差和反演结果有所差异,同等条件下 565、865 nm 波段的 RI 以及 865 nm 波段的

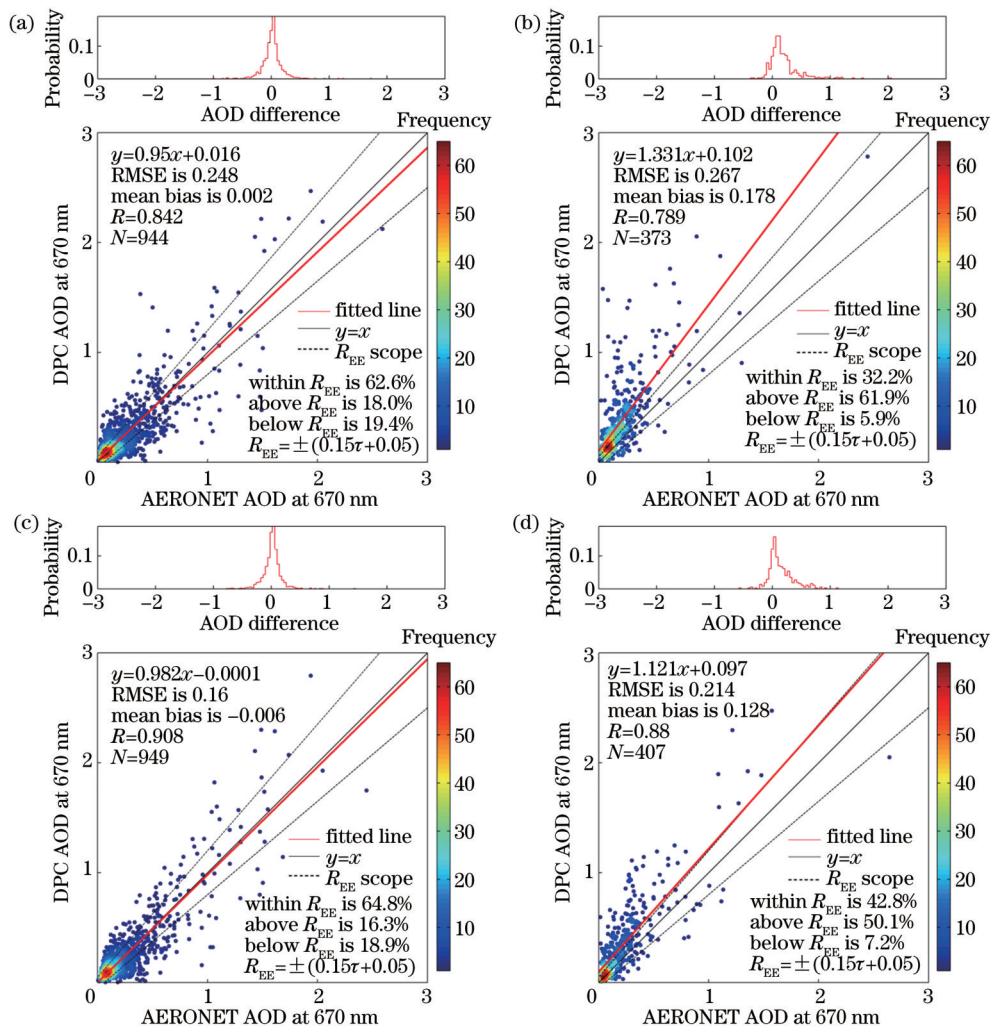


图4 DPC与POLDER在山区与非山区的AOD反演结果散点图。(a)非山区,DPC;(b)山区,DPC;(c)非山区,POLDER;(d)山区,POLDER

Fig. 4 Scatter diagrams of retrieved AODs from DPC and POLDER in mountain and non-mountain area. (a) Non-mountain, DPC; (b) mountain, DPC; (c) non-mountain, POLDER; (d) mountain, POLDER

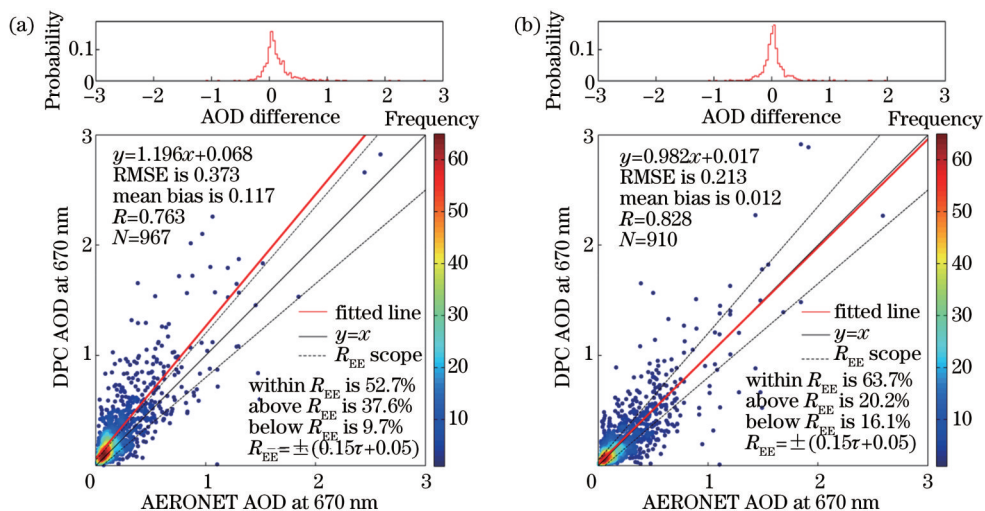


图5 DPC的AOD反演结果散点分布图。(a)仅使用强度;(b)同时使用强度与偏振观测信息

Fig. 5 Scatter diagrams of retrieved AODs from DPC. (a) Only use intensity information; (b) use intensity and polarization information

RP相较POLDER及DPC其他波段要差一些。由于POLDER并没有在同等条件下表现出明显的差异,因此,这种现象的出现与DPC的L1级数据有关。虽然DPC在865 nm波段的AOD误差较大,但AOD的精度在670 nm波段却很优异。由于所有波段共同参与反演,相互之间会有一定的约束,在865 nm波段出现较大误差的情况下DPC依然展现出了较好的反演效果,表明DPC在气溶胶遥感中有较大的潜力。

大散射角情况(后向散射)下,辐射传输模型的模拟精度会降低,进而影响反演精度。在实际的多角度反演中,去除大散射角后反演精度的提升效果并不显著,这是因为:1)大散射角数量较少,对反演的总体影响较小;2)在多角度观测情况下,受其他观测角度的约束,大散射角的影响有所降低。

引入偏振信息后,DPC气溶胶反演精度提升明显。在多角度遥感条件下,地表和气溶胶模型对反演结果的影响较大,偏振信息在估计地表和气溶胶模型方面可以补充强度信息的不足进而提升反演的精度。

DPC和POLDER在山区的反演精度均低于非山区,山区复杂的观测条件导致山区气溶胶反演精度较低,这也给后续相关传感器的研制和算法设计提出了要求。同等条件下,DPC在非山区的反演结果与POLDER接近,但在山区差别较大。DPC的空间分辨率较POLDER要高,虽然在反演过程中通过像元聚合使得反演结果的空间分辨率接近,但是由于山区地表的复杂性,像元聚合方法、几何关系重构、地气耦合等多种因素会影响气溶胶反演结果,这也将是山区气溶胶遥感需要解决的问题。

参 考 文 献

- [1] Chen C, Dubovik O, Schuster G L, et al. Multi-angular polarimetric remote sensing to pinpoint global aerosol absorption and direct radiative forcing[J]. *Nature Communications*, 2022, 13(1): 1-11.
- [2] Guo J P, Su T N, Chen D D, et al. Declining summertime local-scale precipitation frequency over China and the United States, 1981-2012: the disparate roles of aerosols[J]. *Geophysical Research Letters*, 2019, 46(22): 13281-13289.
- [3] 陈洪滨,范学花,夏祥鳌.大气气溶胶的卫星遥感及其在气候和环境研究中的应用[J].*大气科学*,2018,42(3): 621-633.
Chen H B, Fan X H, Xia X A. Review of satellite remote sensing of atmospheric aerosols and its applications in climate and environment studies[J]. *Chinese Journal of Atmospheric Sciences*, 2018, 42(3): 621-633.
- [4] 王涛,周川杰,易维宁,等.基于大气校正提升亚米级卫星影像质量[J].*光学学报*,2021,41(11): 1101002.
Wang T, Zhou C J, Yi W N, et al. Improving sub-meter satellite image quality based on atmospheric correction[J]. *Acta Optica Sinica*, 2021, 41(11): 1101002.
- [5] Partanen A I, Landry J S, Matthews H D. Climate and health implications of future aerosol emission scenarios[J]. *Environmental Research Letters*, 2018, 13(2): 024028.
- [6] 毛前军,金穗穗.2009年至2018年全球气溶胶光学厚度时空分布特性研究[J].*激光与光电子学进展*,2021,58(3): 0301001.
Mao Q J, Jin S S. Investigation of spatial and temporal distribution characteristics of global aerosol optical depth from
- [7] 2009 to 2018[J]. *Laser & Optoelectronics Progress*, 2021, 58(3): 0301001.
- [8] Mishchenko M I, Travis L D. Satellite retrieval of aerosol properties over the ocean using polarization as well as intensity of reflected sunlight[J]. *Journal of Geophysical Research: Atmospheres*, 1997, 102(D14): 16989-17013.
- [9] Deuzé J L, Bréon F M, Devaux C, et al. Remote sensing of aerosols over land surfaces from POLDER-ADEOS-1 polarized measurements[J]. *Journal of Geophysical Research: Atmospheres*, 2001, 106(D5): 4913-4926.
- [10] 段民征,吕达仁.利用多角度POLDER偏振资料实现陆地上空大气气溶胶光学厚度和地表反照率的同时反演 I.理论与模拟[J].*大气科学*,2007,31(5): 757-765.
Duan M Z, Lü D R. Simultaneously retrieving aerosol optical depth and surface albedo over land from POLDER's multi-angle polarized measurements. I: theory and simulations[J]. *Chinese Journal of Atmospheric Sciences*, 2007, 31(5): 757-765.
- [11] Li X, Strahler A H. Geometric-optical bidirectional reflectance modeling of the discrete crown vegetation canopy: effect of crown shape and mutual shadowing[J]. *IEEE Transactions on Geoscience and Remote Sensing*, 1992, 30(2): 276-292.
- [12] Maignan F, Bréon F M, Fédele E, et al. Polarized reflectances of natural surfaces: spaceborne measurements and analytical modeling[J]. *Remote Sensing of Environment*, 2009, 113(12): 2642-2650.
- [13] 提汝芳,樊依哲,黄红莲,等.基于高分五号卫星DPC和AERONET站点数据的地表BPDF模型对比分析[J].*光学学报*,2022,42(18): 1828003.
Ti R F, Fan Y Z, Huang H L, et al. Comparative analysis of BPDF land surface models based on DPC measurements of Gaofen-5 satellite and data of AERONET sites[J]. *Acta Optica Sinica*, 2022, 42(18): 1828003.
- [14] Dubovik O, Herman M, Holdak A, et al. Statistically optimized inversion algorithm for enhanced retrieval of aerosol properties from spectral multi-angle polarimetric satellite observations[J]. *Atmospheric Measurement Techniques*, 2011, 4(5): 975-1018.
- [15] Hasekamp O P, Litvinov P, Butz A. Aerosol properties over the ocean from PARASOL multiangle photopolarimetric measurements[J]. *Journal of Geophysical Research*, 2011, 116(D14): D14204.
- [16] Cheng T, Gu X, Xie D, et al. Aerosol optical depth and fine-mode fraction retrieval over East Asia using multi-angular total and polarized remote sensing[J]. *Atmospheric Measurement Techniques*, 2012, 5(3): 501-516.
- [17] Xie D H, Cheng T H, Zhang W, et al. Aerosol type over East Asian retrieval using total and polarized remote sensing[J]. *Journal of Quantitative Spectroscopy and Radiative Transfer*, 2013, 129(11): 15-30.
- [18] Wang Z T, Chen L F, Li Q, et al. Retrieval of aerosol size distribution from multi-angle polarized measurements assisted by intensity measurements over East China[J]. *Remote Sensing of Environment*, 2012, 124: 679-688.
- [19] Dubovik O, Li Z Q, Mishchenko M I, et al. Polarimetric remote sensing of atmospheric aerosols: instruments, methodologies, results, and perspectives[J]. *Journal of Quantitative Spectroscopy and Radiative Transfer*, 2019, 224: 474-511.
- [20] Cheng T H, Gu X F, Xie D H, et al. Simultaneous retrieval of aerosol optical properties over the Pearl River Delta, China using multi-angular, multi-spectral, and polarized measurements [J]. *Remote Sensing of Environment*, 2011, 115(7): 1643-1652.
- [21] 郑逢勋,侯伟真,李正强.高分五号卫星多角度偏振相机最优化估计反演:角度依赖与后验误差分析[J].*物理学报*,2019,68(4): 040701.
Zheng F X, Hou W Z, Li Z Q. Optimal estimation retrieval for directional polarimetric camera onboard Chinese Gaofen-5 satellite: an analysis on multi-angle dependence and a posteriori

- error[J]. Acta Physica Sinica, 2019, 68(4): 040701.
- [21] Li Z Q, Xie Y S, Hou W Z, et al. Global haze aerosol distribution: a direct view by Geofen-5 satellite with 3.3 km spatial resolution[EB/OL]. (2019-06-17)[2022-11-12]. <https://arxiv.org/abs/1906.09911>.
- [22] Wang H, Sun X B, Yang L K, et al. Aerosol retrieval algorithm based on adaptive land - atmospheric decoupling for polarized remote sensing over land surfaces[J]. Journal of Quantitative Spectroscopy and Radiative Transfer, 2018, 219: 74-84.
- [23] Wang H, Zhai Y C, Zhao M R, et al. Evaluation of aerosol optical depth products from multiangular and polarized satellite measurements over mountainous areas[J]. IEEE Transactions on Geoscience and Remote Sensing, 2022, 60: 4109810.
- [24] Lenoble J, Herman M, Deuzé J L, et al. A successive order of scattering code for solving the vector equation of transfer in the earth's atmosphere with aerosols[J]. Journal of Quantitative Spectroscopy and Radiative Transfer, 2007, 107(3): 479-507.
- [25] Eck T F, Holben B N, Reid J S, et al. Wavelength dependence of the optical depth of biomass burning, urban, and desert dust aerosols[J]. Journal of Geophysical Research: Atmospheres, 1999, 104(D24): 31333-31349.

Aerosol Inversion Test of Directional Polarimetric Camera Based on Posterior Error Analysis

Wang Han^{1*}, Sun Xiaobing², Zhao Meiru^{3**}, Qin Kai¹

¹School of Environment and Spatial Informatics, China University of Mining and Technology, Xuzhou 221116, Jiangsu, China;

²Anhui Institute of Optics and Fine Mechanics, Chinese Academy of Sciences, Hefei 230031, Anhui, China;

³School of Geography and Tourism, Anhui Normal University, Wuhu 241000, Anhui, China

Abstract

Objective Aerosols are an important component of the earth's atmospheric system and exert significant effects on radiation forcing, meteorology, environment, quantitative remote sensing, and human health. The demand for high-precision aerosol products in scientific research and social production continues to grow. Multi-spectral, multi-angular, and polarization observations can better achieve global aerosol detection. The directional polarimetric camera (DPC) sensor is currently carried on satellites Gaofen-5A, Gaofen-5B, and the atmospheric environment monitoring satellite to conduct global atmospheric environment monitoring. DPC can obtain observation data from three polarization bands and five non-polarization bands, with a minimum of nine and a maximum of seventeen angles. Currently, there is an urgent need for DPC to provide aerosol products of reliable scientific and application significance. The posterior error analysis in inversion results is an important tool in testing DPC performance.

Methods The entire process of our research includes data matching, aerosol inversion, and analysis of error dependence on wavelength and scattering angle. At the same time, the DPC and polarization and directionality of the earth's reflectance (POLDER) results are compared in the same conditions. First, the satellite transit time over the aerosol robotic network (AERONET) site and the pixel where the AERONET site is located are determined through spatio-temporal matching, and the matching results are trimmed and stored. Second, the generalized retrieval of aerosol and surface properties (GRASP) algorithm is adopted to retrieve the matched DPC and POLDER data. To test the performance of DPC and ensure the comparison in the same conditions, we employ the common band of DPC and POLDER to retrieve both data. Third, the successful order of scattering (SOS) radiation transfer program is leveraged to conduct forward simulation with the inversion results of DPC and POLDER as inputs. Compared with the observed values, the inversion residuals for each band and angle are obtained (RI and RP representing intensity and polarization residuals, respectively), and the distribution of RI and RP in each band is analyzed. Then, the multi-band aerosol optical depth (AOD) observed by AERONET is employed as the real value, and the error distribution differences between DPC and POLDER retrieved AOD relative to AERONET products are compared in the same conditions. Finally, the influence of scattering angles is analyzed. Satellite observation scattering angles are mostly distributed between 100° and 175°. The distribution of RI and RP at 5° intervals is studied, and a comparative analysis of the scattering angle dependence of RI and RP is conducted.

Results and Discussions First, the variation of the inversion residual with the wavelength is analyzed. The results show that RI and RP of DPC and POLDER are both at lower levels, which are about 10×10^{-3} and 10×10^{-4} , respectively. The overall distribution of RI and RP from DPC and POLDER is relatively centralized. But for RI@565, RI@865, and RP@865 of DPC, the error bar of them is relatively large (Fig. 1). The inversion results of DPC are generally in good agreement with AERONET, reflecting the DPC ability in aerosol observation. However, AOD@865 is seriously

overvalued (Table 2). Second, the variation of inversion residual with scattering angle is also analyzed. We find that the mean values of RI and RP in mountain areas are higher than those in non-mountain areas, with relatively discrete RI and RP. In non-mountain areas, RI and RP are relatively concentrated, but the standard deviation is large when the scattering angle is greater than 160° . The angular characteristics of the DPC and POLDER residuals are relatively consistent, without significant differences (Figs. 2 and 3). Third, after discussing the inversion results of the mountain and non-mountain areas, the inversion ability of DPC in non-mountain areas is proven to be close to POLDER, while in mountain areas it lags behind POLDER (Fig. 4). Fourth, the influence of polarization on AOD inversion is discussed. It is found that polarization information can significantly improve the AOD inversion effect, with correlation increasing from 0.763 to 0.808, RMSE decreasing from 0.373 to 0.213, mean bias decreasing from 0.117 to 0.012, and the proportion of falling into the expected error section R_{EE} increasing from 44.4% to 55.7% (Fig. 5). Cross comparison between Figs. 4 and 5 shows that deducting large scattering angles in the inversion process can improve the inversion effect, but the effect is not obvious.

Conclusions First, although the error of AOD@865 from DPC is large, it is excellent at 670 nm band. Due to the common participation of all wavelengths in retrieval, there will be certain constraints between them. AOD@670 still exhibits good results even when there is a large error in the 865 nm band, which indicates that DPC has great potential in aerosol remote sensing. Second, in the case of large scattering angles, the simulation accuracy of the radiation transfer model will decrease, thereby affecting the inversion accuracy. However, due to the small number of large scattering angles and multi-angular constraints, the effect of large scattering angles is reduced. Therefore, in practical multi-angle inversion, large scattering angles do not significantly improve the inversion accuracy. Third, polarization information exerts a significant influence on improving aerosol retrieval accuracy. In multi-angular remote sensing, polarization information can supplement intensity information in estimating surface and aerosol models, thereby improving the retrieval accuracy. Fourth, the DPC inversion in non-mountain areas is similar to that of POLDER, but there is a significant difference in mountain areas. Since the spatial resolution of DPC is higher than that of POLDER, many factors including pixel aggregation, geometric reconstruction, and land surface-atmosphere coupling can affect aerosol retrieval results. This will also be a problem to be addressed in aerosol remote sensing of mountainous areas.

Key words remote sensing and sensors; aerosol; polarization; directional polarimetric camera